

Supporting Information

**High-efficiency photocatalytic degradation of rhodamine 6G
by organic semiconductor tetrathiafulvalene in weak acid-
base environment**

Yukun Cui,^a Yi Li,^{*a,b} Yaru Liu,^a Denghui Shang,^a Yu Liu,^{*a} Liangbo Xie,^a

Sihui Zhan,^{*c} and Wenping Hu,^{a,b}

^a Tianjin Key Laboratory of Molecular Optoelectronic Sciences, Department of Chemistry, School of Science, Tianjin University & Collaborative Innovation Center of Chemical Science and Engineering (Tianjin), Tianjin 300072, China.

^b Joint School of National University of Singapore and Tianjin University, Fuzhou International Campus, Tianjin University, Binhai New City, Fuzhou 350207, China.

^c College of Environmental Science and Engineering, Nankai University, Tianjin 300071, China.

Table of Contents

Experimental	S3-5
Fig. S1 SEM images of TTF (a, b, c), XRD pattern of TTF (d).	S6
Fig. S2 Transient photocurrent response spectrum (a) and UV-vis DRS (b) of TTF.	S7
Fig. S3 The concentrations of H ₂ O ₂ at different pH values in Rh6G degradation process.	S8
Fig. S4 (a) The UV-vis spectra of TTF aqueous solution with different pH under irradiation for 0 and 60 min. (b) Comparison with different pH values of TTF aqueous solutions after irradiation for 60 min.	S9
Fig. S5 The Raman spectra (a) and FT-IR spectra (b) of TTF before and after photocatalytic reaction.	S10
Fig. S6 The HPLC-MS spectrometry of TTF before and after photocatalytic reaction.	S11
Fig. S7 Possible degradation pathways of Rh6G.	S12
Table S1 The intermediates generated during the photocatalytic degradation process of Rh6G.	S13-14
References	S15

Experimental

Reagents

Tetrathiafulvalene ($C_6H_4S_4$, 98.5%) was purchased from Beijing J&K Scientific Ltd. Cerium (IV) sulfate hydrate ($Ce(SO_4)_2 \cdot H_2O$, 99.99%) was supplied by Bide Pharmatech Ltd. L-histidine ($C_6H_9N_3O_2$, 99%) was purchased from Shanghai Rhawn Chemical Technology Co., Ltd. Rhodamine 6G ($C_{28}H_{31}N_2O_3Cl$, BS) and 2,2,6,6-tetramethylpiperidine-1-oxyl (TEMPO, 98%) were supplied by Aladdin Biochemical Technology Co., Ltd. Catalase was obtained from Nanjing Duly Biotechnology Co., Ltd. Superoxide dismutase (SOD) was acquired from Tianjin Haoshengjie Biotechnology Co., Ltd. 2,2,6,6-Tetramethylpiperidine (TEMP) and 5-dimethyl-1-pyrroline-N-oxide (DMPO) were acquired from Sigma-Aldrich. All the above chemicals were used without further purification.

Characterizations

The morphology of the sample was observed by field emission scanning electron microscope (SEM, JEOL-6700 FESEM, Japan). Power X-ray diffraction (XRD) pattern was conducted on an X-ray diffractometer (Rigaku D/Max 2200PC, Japan) with a Cu $K\alpha$ radiation ($\lambda = 0.15418 \text{ \AA}$) to analyze the crystal structure of sample. The optical performance of sample was detected by UV-vis diffuse reflectance spectrum (DRS) equipped with UV-vis spectrophotometer (Shimadzu, UV-3600, Japan). The concentration of pollutant was obtained on ultraviolet (UV-vis) spectrophotometry (Thermo Fisher Scientific, GENESYS 180, USA). The Fourier transform infrared spectra (FT-IR) was investigated by FT-IR spectroscopy (Thermo Nicolet iS5, USA) with the KBr disk method. Raman spectrum was recorded on Thermo Scientific DXR2

spectrometer under an excitation wavelength of 633 nm. The intermediates products were determined by high performance liquid chromatography-quadrupole-time of flight tandem mass spectrometer (HPLC-MS, Bruker Daltonics Inc, USA) equipped with ESI source. To determine the species of radicals, the signals of TEMP-¹O₂, DMPO-[•]OH, DMPO-[•]O₂⁻ and TEMPO were obtained on electron paramagnetic resonance (EPR) spectrometer (Bruker, A300-10/12, Germany).

Electrochemical and photoelectrochemical measurements

Rotating disk electrode (RDE) measurement was determined by electrochemical workstation (CHI 760D, Chenhua, China) with a three-electrode cell. The linear sweep voltammetry (LSV) curves were observed in oxygen-saturated 0.1 mol·L⁻¹ phosphate buffer solution (pH = 7) at a scan rate of 5 mV·s⁻¹. The catalyst-coated glassy carbon electrode (GCE), Ag/AgCl electrode and graphite bar were used as working electrode, reference electrode and counter electrode, respectively.

The Koutecky-Levich (K-L) plots were obtained at different electrode potentials. And taking advantage of the following Eq. (S1-S2), the number of electrons transferred (*n*) was derived by linear regression of the plot.

$$\frac{1}{i} = \frac{1}{i_{\text{lim}}} + \frac{1}{i_{\text{k}}} \quad (\text{Eq. S1})$$

$$i_{\text{lim}} = 0.62nFA\omega^{\frac{1}{2}}\nu^{-\frac{1}{2}}D_0^{\frac{2}{3}}C_0 \quad (\text{Eq. S2})$$

where *i* is the recorded current, *i_k* is the kinetic current, *i_{lim}* is the limiting current, *F* is the Faraday constant (96485 C·mol⁻¹), *A* is the electrode area (*A* = 0.196 cm²), *ω* is the angular rotation rate of the electrode, *ν* is the kinetic viscosity of water (0.01

$\text{cm}^2\cdot\text{s}^{-1}$), D_0 is the diffusion coefficient of O_2 ($2.7 \times 10^{-5} \text{ cm}^2\cdot\text{s}^{-1}$), C_0 is the bulk concentration of O_2 in aqueous solution ($1.3 \times 10^{-6} \text{ mol}\cdot\text{cm}^{-3}$), respectively.¹

The photocurrent response was measured by electrochemical workstation (CHI 660D, Chenhua, China) in three-electrode system. The test was performed in $0.5 \text{ mol}\cdot\text{L}^{-1}$ sodium sulfate solution with light on or off. And, the catalyst-coated fluorine-doped tin oxide (FTO) electrode, Pt sheet and saturated calomel electrode (SCE) were served as working electrode, counter electrode and reference electrode, respectively.

Degradation procedure

Rh6G ($10 \text{ mg}\cdot\text{L}^{-1}$) was selected as the target pollutant to estimate the photo-degradation performance under visible light irradiation (300 W xenon lamp, CEL-HXF300, $\lambda > 420 \text{ nm}$). 5 mg grinding TTF was added to 50 mL contaminant solution under constant stirring. The pH value of the solution was adjusted by $0.1 \text{ mol}\cdot\text{L}^{-1}$ NaOH or $0.1 \text{ mol}\cdot\text{L}^{-1}$ H_2SO_4 solution. Oxygen was constantly injected throughout the degradation experiment. The mixture was stirred for 30 min under dark before irradiation to ensure TTF uniformly dispersed in solution. During the degradation process, 2 mL of the sample solution was extracted at given time interval and analyzed by UV-vis spectrophotometer at maximum absorption wavelength (526 nm for Rh6G).

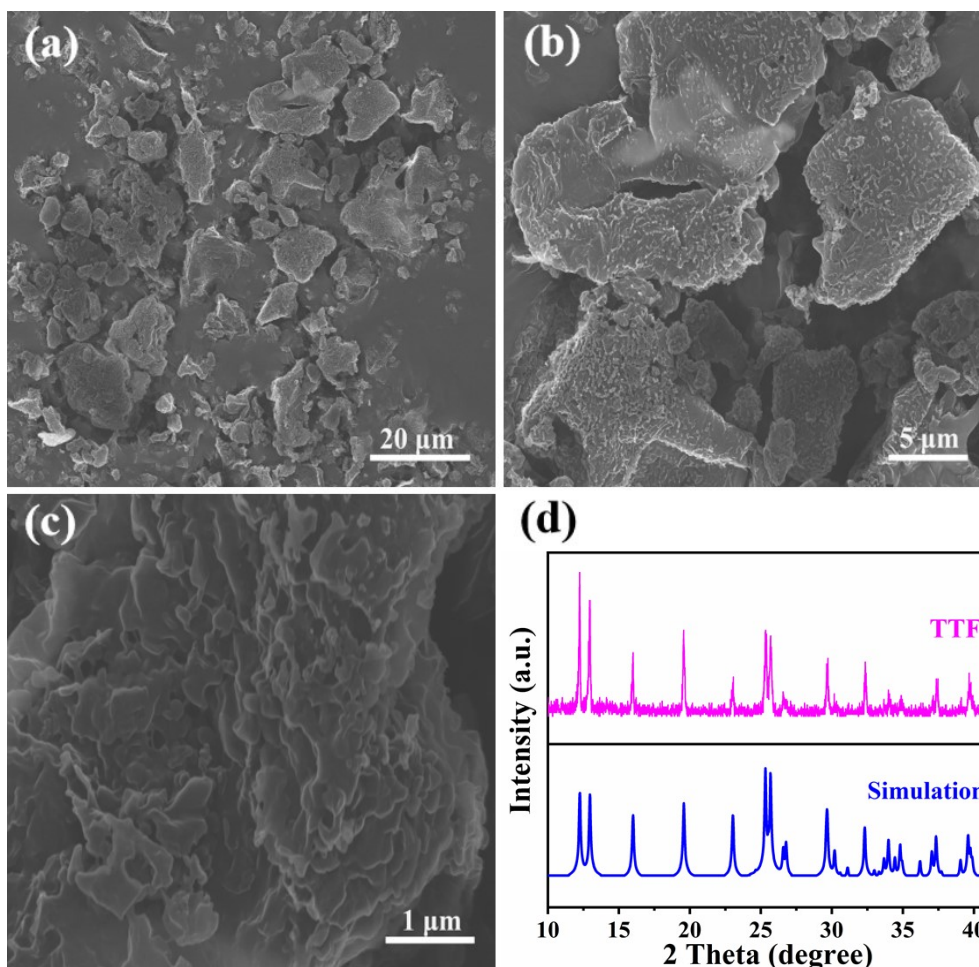


Fig. S1. SEM images of TTF (a, b, c), XRD pattern of TTF (d).

As shown in Fig. S1d, the diffraction peaks at 2θ of 12.2° , 12.9° , 16.0° , 19.6° , 25.2° , 25.6° , 29.7° , 32.3° , 37.4° and 39.7° corresponded well to planes of (100), (002), (10), (102), (110), (10), (202), (20), (300) and (006), which were consistent with the α -TTF crystalline simulated peaks. It indicated that TTF used in this experiment was α -TTF, which belonged to the space group $P2_1/c$.²

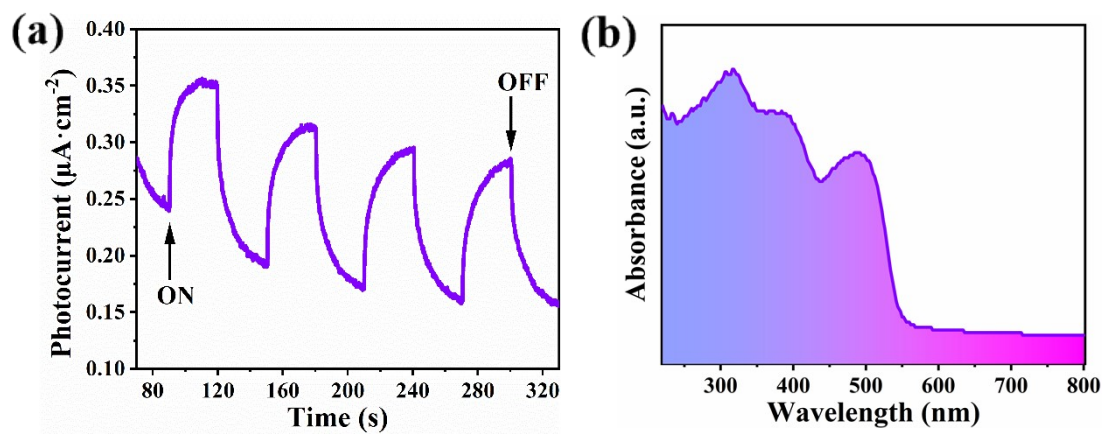


Fig. S2. Transient photocurrent response spectrum (a) and UV-vis DRS (b) of TTF.

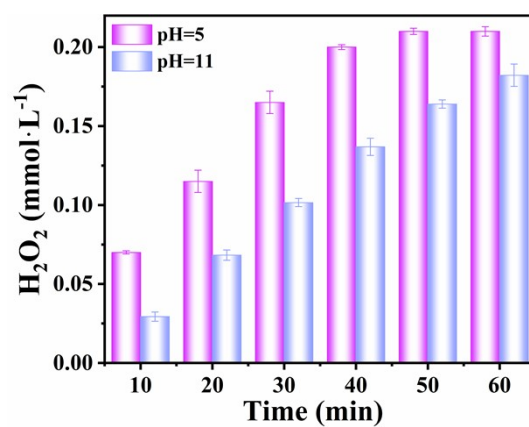


Fig. S3. The concentrations of H_2O_2 at different pH values in Rh6G degradation process.

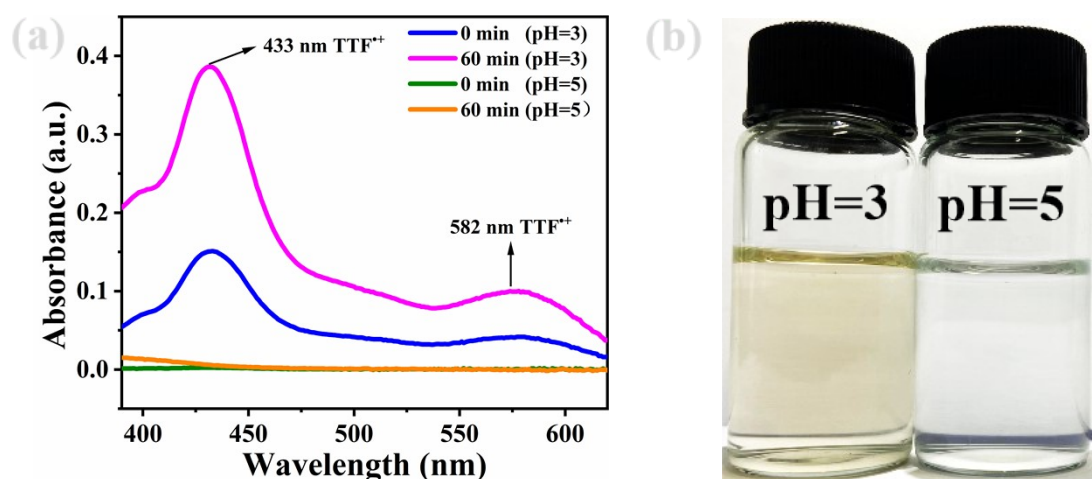


Fig. S4. (a) The UV-vis spectra of TTF aqueous solution with different pH under irradiation for 0 and 60 min. (b) Comparison with different pH values of TTF aqueous solutions after irradiation for 60 min.

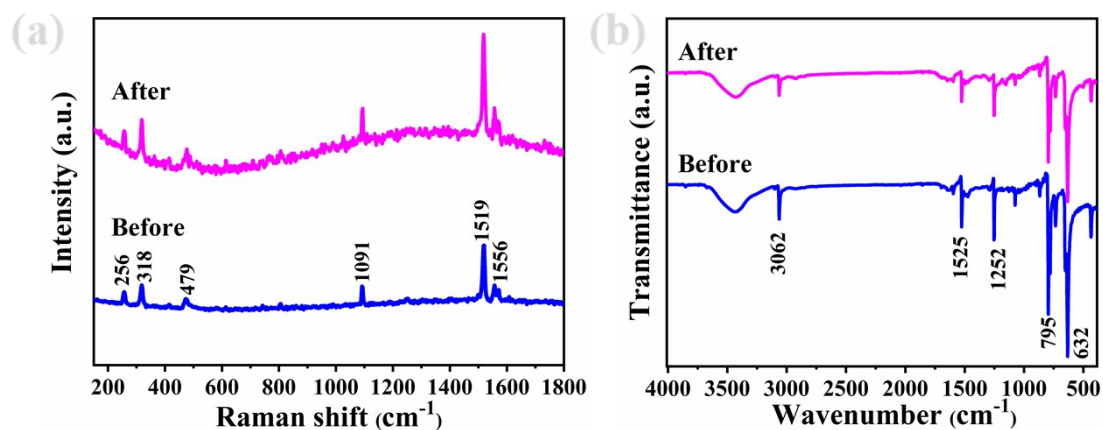


Fig. S5. The Raman spectra (a) and FT-IR spectra (b) of TTF before and after photocatalytic reaction.

As depicted in Fig. S5a, the peaks at 1519 and 1556 cm⁻¹ corresponded to C=C stretching vibration. The peak at 1091 cm⁻¹ was attributed to the in-plane C-H bending mode and the bands at 479, 318 and 256 cm⁻¹ were ascribed to skeletal stretches and bends.³ In Fig. S5b, the peaks at 3062, 1525 and 795 cm⁻¹ were C-H stretching vibration, C=C stretching vibration and C-S stretching, respectively.⁴ In addition, the peaks at 1252 and 632 cm⁻¹ were assigned to the C-H bending and C-H out of plane bending, respectively.⁵

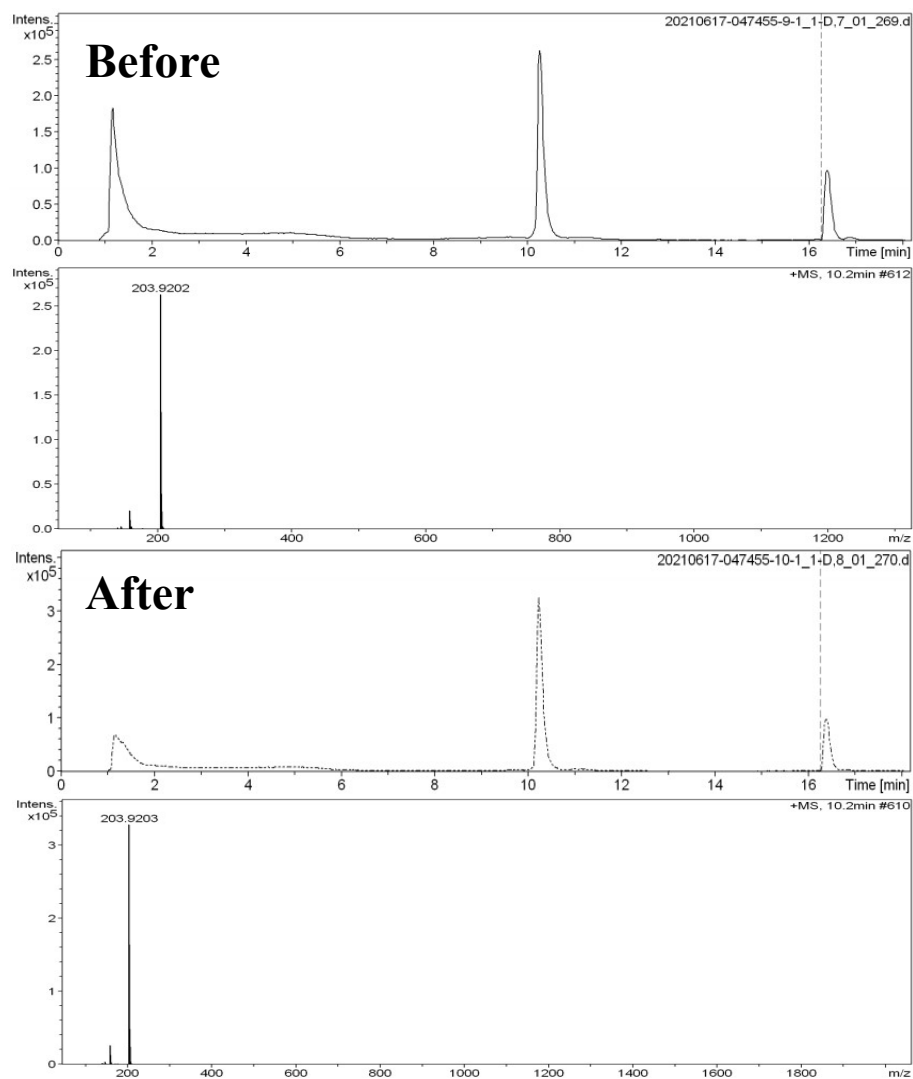


Fig. S6. The HPLC-MS spectrometry of TTF before and after photocatalytic reaction.

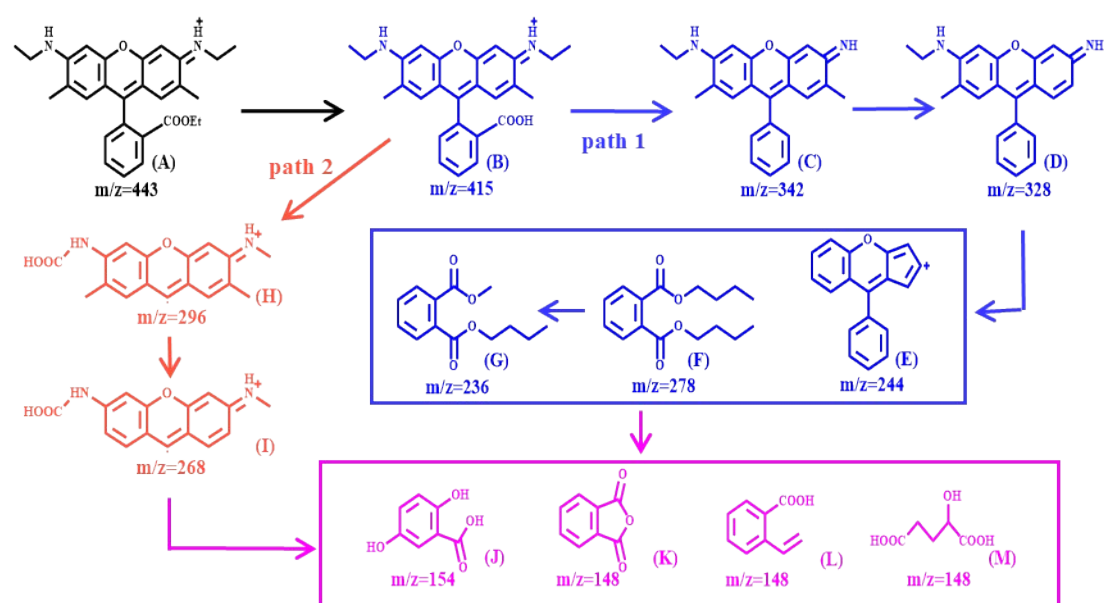
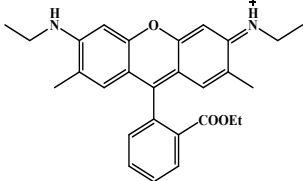
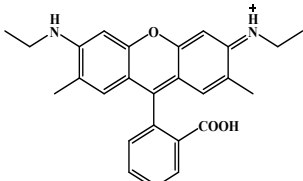
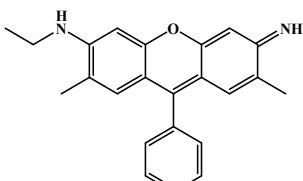
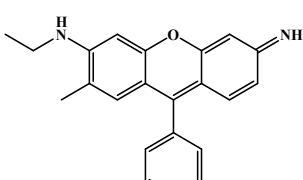
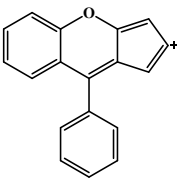
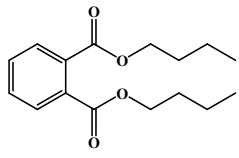
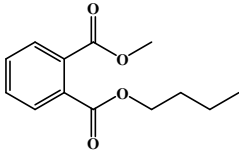
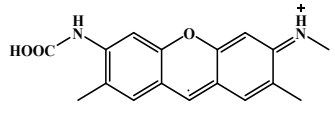
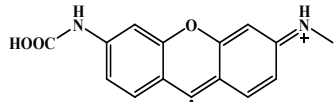
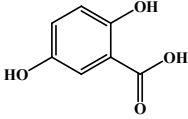
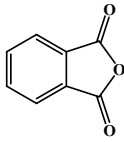
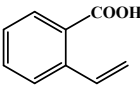
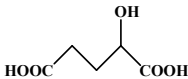


Fig. S7. Possible degradation pathways of Rh6G.

In the original solution before degradation, Rh6G was observed merely at $m/z = 443$. In Fig. S7 (ESI[†]), two possible degradation routes of Rh6G were proposed. The Rh6G molecule was subject to an esterification reaction, converting the ester group to a carboxylic acid and generating a possible by-product ($m/z = 415$). In pathway 1, the generated radicals could attack the carbon atom with high negative density charge, which led to the loss of the ethyl group, and then the molecule was stripped of carboxylic acid to obtain by-product ($m/z = 342$). Subsequently, the methyl group was eliminated to get by-product ($m/z = 328$), which further degraded to molecules ($m/z = 244$, $m/z = 278$, $m/z = 236$). In pathway 2, the possible degradation by-product corresponding to m/z value of 296 could be formed in the N-de-ethylation, carboxylation, and demethylation process, followed by the loss of two methyl groups to generate product ($m/z = 268$).^{6,7} In both pathway 1 and 2, the product fragmented into small molecules ($m/z = 154$ and $m/z = 148$), which were eventually converted to smaller molecules.^{8,9}

Table S1. The intermediates generated during the photocatalytic degradation process of Rh6G.

Compounds	Molecular formula	Structural formula	m/z
A	$C_{28}H_{31}N_2O_3^+$		443
B	$C_{26}H_{27}N_2O_3^+$		415
C	$C_{23}H_{22}N_2O$		342
D	$C_{22}H_{20}N_2O$		328
E	$C_{18}H_{14}O^+$		244
F	$C_{16}H_{22}O_4$		278
G	$C_{13}H_{16}O_4$		236
H	$C_{17}H_{16}N_2O_3^+$		296
I	$C_{15}H_{14}NO^+$		268

J	$C_7H_6O_4$		154
K	$C_8H_4O_3$		148
L	$C_9H_8O_2$		148
M	$C_5H_8O_5$		148

References

1. J. Xiao, Q. Liu, M. Song, X. R. Li, Q. Li and J. K. Shang, *Water Res.*, 2021, **198**, 117125.
2. H. Jiang, X. J. Yang, Z. D. Cui, Y. C. Liu, H. X. Li, W. P. Hu, Y. Q. Liu and D. B. Zhu, *Appl. Phys. Lett.*, 2007, **91**, 123505.
3. A. J. Berlinsky, Y. Hoyano and L. Weiler, *Chem. Phys. Lett.*, 1977, **45**, 419-421.
4. V. Mukherjee and T. P. Yadav, *Spectroc. Acta Pt. A Molec. Biomolec. Spectr.*, 2017, **176**, 18-29.
5. V. Mukherjee and D. P. Ojha, *Spectroc. Acta Pt. A Molec. Biomolec. Spectr.*, 2020, **231**, 117849.
6. S. Rajoriya, S. Bargole and V. K. Saharan, *Ultrason. Sonochem.*, 2017, **34**, 183-194.
7. T. S. Natarajan, M. Thomas, K. Natarajan, H. C. Bajaj and R. J. Tayade, *Chem. Eng. J.*, 2011, **169**, 126-134.
8. G. Sharma, D. D. Dionysiou, S. Sharma, A. Kumar, A. a. H. Al-Muhtaseb, M. Naushad and F. J. Stadler, *Catal. Today*, 2019, **335**, 437-451.
9. Y. Liu, H. G. Guo, Y. L. Zhang, X. Cheng, P. Zhou, G. C. Zhang, J. Q. Wang, P. Tang, T. L. Ke and W. Li, *Sep. Purif. Technol.*, 2018, **192**, 88-98.